C. R. Geoscience 343 (2011) 584–590

Contents lists available at ScienceDirect

Comptes Rendus Geoscience

www.sciencedirect.com

Internal geophysics (Physics of Earth's interior)

Two-dimensional sensitivity kernels for cross-correlation functions of background surface waves

Noyaux de sensibilité bi-dimensionnelle pour fonctions de corrélations croisées d'ondes de surface

Kiwamu Nishida

Earthquake Research Institute, University of Tokyo, Tokyo, Japan

ARTICLE INFO

Article history:
Received 1 September 2010
Accepted after revision 1 March 2011
Available online 31 May 2011

Written on invitation of the Editorial Board

Mots-clés :
Interférométrie
Noyau de sensibilité
Tomographie en bruit ambiant

Keywords:
Interferometry
Sensitivity kernel
Ambient noise tomography

ABSTRACT

Ambient noise tomography has now been applied at scales ranging from local to global. To discuss the theoretical background of the technique, a simple form of a two-dimensional (2-D) Born sensitivity kernel was developed at a finite frequency for a cross-correlation function (CCF) of background surface waves. The use of far field representations of a Green's function and a CCF in a spherically symmetric Earth model, assuming a homogeneous source distribution, is an efficient approach to the calculation of phase sensitivity kernels. The forms of a phase sensitivity kernel for major and minor arc propagations are the same as those for phase-velocity measurements of earthquake data. This result indicates the validity of ambient noise tomography under the given assumptions; however, the kernels are not equivalent in the case of an inhomogeneous source distribution.

RÉSUMÉ

La tomographie à partir du bruit ambiant a, à présent, été appliquée à des échelles à la fois locales et globales . Pour discuter des fondements théoriques de la technique, une simple forme de noyau de sensibilité de Born à 2D et à fréquence finie a été développée pour une fonction de corrélation (CCF) d'un bruit consistant en ondes de surface. L'utilisation de représentations en champ lointain d'une fonction de Green et d'une CCF dans un modèle de Terre à symétrie sphérique, en supposant une distribution de source homogène, est une approche efficace pour le calcul de noyaux de sensibilité de la vitesse de phase. Les formes des noyaux de sensibilité pour les propagations le long d'arcs majeurs et mineurs sont les mêmes que celles qu'on observe dans les mesures de vitesse de phase avec les observations des séismes. Ce résultat indique la validité de la tomographie à partir du bruit ambiant dans les hypothèses données ici; cependant, les noyaux ne sont pas équivalents dans le cas d'une distribution inhomogène de sources.

1. Introduction

Shapiro et al. (2005) performed a cross-correlation analysis of long sequences of ambient seismic noise at around 0.1 Hz to obtain a group-velocity anomaly of Rayleigh

Email address: knishida@eri.u-tokyo.ac.jp.

1631-0713/$ – see front matter
doi:10.1016/j.crte.2011.02.004

waves due to the lateral heterogeneity of the crust in southern California. The authors inverted the measured anomalies to obtain a group-velocity map, employing a method that is now referred to as 'ambient noise tomography'. The obtained group–velocity map at short periods (7.5–15 s) shows a striking correlation with the geologic structure.

Recently, phase velocity anomalies have also been measured using dense networks of seismic stations (Bensen et al., 2007). The anomalies are inverted to yield the three-dimensional S-wave velocity structure in the crust and in the uppermost mantle (Bensen et al., 2009; Nishida et al., 2008). The tomographic method was now been applied at scales ranging from local to global (Nishida et al., 2009).

The theoretical basis of cross-correlation analysis is the fact that a cross-correlation function (CCF) between a pair of stations provides the wave propagation between them (Snieder, 2004), as with the Green's function. Assuming that a CCF has sensitivity along the ray path between a pair of stations (Lin et al., 2009), the measured phase or group velocity anomalies can be inverted to obtain maps of phase or group velocity. The ray approximation is justified by the high-frequency limit of the phase–velocity sensitivity kernel. The kernels for earthquake data have been evaluated by many researchers (Spetzler et al., 2002; Yoshizawa and Kennett, 2005; Zhou et al., 2004), but only one previous study has investigated ambient noise tomography (Tromp et al., 2010).

In the present study, a form of a two-dimensional (2-D) Born sensitivity kernel is obtained for a CCF, assuming the stochastic excitation of surface waves. For simplicity, potential representation is used for surface waves. The Born sensitivity kernel is then calculated in a spherically symmetric Earth model assuming a homogeneous source distribution. A simple expression of phase sensitivity kernels is derived from the Born sensitive kernel based on the Rytov approximation with the far-field approximation of a Green's function and a CCF.

2. Theory of a synthetic cross spectrum of background surface waves between a pair of stations

For estimation of the sensitivity kernels, this section develops the theory of a synthetic CCF of background surface waves between a pair of stations.

It is assumed that a displacement field $\boldsymbol{u}$ can be represented by a fundamental Love wave and a fundamental Rayleigh wave, as follows:

$$\boldsymbol{u} = \boldsymbol{u}_L + \boldsymbol{u}_R. \tag{1}$$

Love and Rayleigh wave displacement fields in laterally, slowing varying media can be written in terms of surface wave potentials (Tanimoto, 1990; Tromp and Dahlen, 1993). The Love wave part $\boldsymbol{u}_L$ and the Rayleigh wave part $\boldsymbol{u}_R$ are given by the surface wave potential χ_α, as follows:

$$\boldsymbol{u}_\alpha = \mathcal{D}_\alpha \chi_\alpha, \tag{2}$$

where the subscript α represents the Love wave (L) or Rayleigh wave (R). The spatial differential operators $\mathcal{D}_R$ and $\mathcal{D}_L$ are respectively defined as follows:

$$\mathcal{D}_R = U(\boldsymbol{r},\omega)\hat{\boldsymbol{r}} + k_R^{-1}(\hat{\boldsymbol{r}},\omega)V(\boldsymbol{r},\omega)\nabla_l \tag{3}$$

$$\mathcal{D}_L = k_L^{-1}(\hat{\boldsymbol{r}},\omega)W(\boldsymbol{r},\omega)(-\hat{\boldsymbol{r}}\times\nabla_l), \tag{4}$$

where ∇_l is the surface gradient operator, $U(\boldsymbol{r},\omega)$ is the local vertical eigenfunction, $V(\boldsymbol{r},\omega)$ is the local radial eigenfunction, and $W(\boldsymbol{r},\omega)$ is the local transverse eigenfunction as a function of surface location $\boldsymbol{r}$, $\hat{\boldsymbol{r}}$ is a unit vector defined on a unit sphere, and $k_\alpha(\hat{\boldsymbol{r}},\omega)$ is the local wavenumber at the angular frequency ω. $k_\alpha(\hat{\boldsymbol{r}},\omega)$ can also be written in terms of the phase velocity $c_\alpha(\hat{\boldsymbol{r}},\omega)$, as follows: $k_\alpha(\hat{\boldsymbol{r}},\omega) = \omega/c_\alpha(\hat{\boldsymbol{r}},\omega)$. The convention for the Fourier transform is that $\exp(-i\omega t)$ appears in the Fourier integral when transforming from the time domain to the frequency domain. The eigenfunctions are normalized following Tromp and Dahlen (1993), as $c_\alpha(\hat{\boldsymbol{r}},\omega)C_\alpha(\hat{\boldsymbol{r}},\omega)I_{1_\alpha}(\hat{\boldsymbol{r}},\omega) = 1$, where $C_\alpha(\hat{\boldsymbol{r}},\omega)$ is the group velocity and $I_{1\alpha}$ is the energy integral.

The surface wave potentials satisfy the inhomogeneous spherical Helmholtz equation of a surface wave (Tromp and Dahlen, 1993), as follows:

$$\nabla_l^2\chi_\alpha(\hat{\boldsymbol{r}},\omega) + \xi_\alpha^2(\hat{\boldsymbol{r}},\omega)\chi_\alpha(\hat{\boldsymbol{r}},\omega) = F_\alpha(\hat{\boldsymbol{r}},\omega), \tag{5}$$

where ξ_α is the following complex wavenumber,

$$\xi_\alpha(\hat{\boldsymbol{r}},\omega) = k_\alpha(\hat{\boldsymbol{r}},\omega) - \frac{\omega}{2Q_\alpha(\hat{\boldsymbol{r}},\omega)C_\alpha(\hat{\boldsymbol{r}},\omega)}i, \tag{6}$$

where Q_α is a quality factor. The equivalent surface traction F_α is defined as follows:

$$F_L(\hat{\boldsymbol{r}},\omega) = -k_L(\hat{\boldsymbol{r}},\omega)W(\boldsymbol{r},\omega)\,f_3(\hat{\boldsymbol{r}},\omega)R^2, \tag{7}$$

$$F_R(\hat{\boldsymbol{r}},\omega) = -(U(\boldsymbol{r},\omega)\,f_1(\hat{\boldsymbol{r}},\omega) + k_R(\hat{\boldsymbol{r}},\omega)V(\boldsymbol{r},\omega)\,f_2(\hat{\boldsymbol{r}},\omega))R^2, \tag{8}$$

where R is the radius of the Earth. Here, f_1 and f_2 are spheroidal components of the equivalent surface traction $\boldsymbol{f}$, and f_3 is a toroidal component of $\boldsymbol{f}$ in the form of $\boldsymbol{f} = \hat{\boldsymbol{r}}f_1 + \nabla_l f_2 - \hat{\boldsymbol{r}}\times\nabla_l f_3$.

A scalar Green's function of Love and Rayleigh waves $G_\alpha(\hat{\boldsymbol{r}},\hat{\boldsymbol{r}}_s,\omega)$ satisfies

$$\nabla_l^2 G_\alpha(\hat{\boldsymbol{r}},\hat{\boldsymbol{r}}_s,\omega) + \xi_\alpha^2 G_\alpha(\hat{\boldsymbol{r}},\hat{\boldsymbol{r}}_s,\omega) = -\delta(\hat{\boldsymbol{r}},\hat{\boldsymbol{r}}_s). \tag{9}$$

A scalar potential function χ_α can be written as

$$\chi_\alpha(\hat{\boldsymbol{r}},\omega) = \int_\Sigma G_\alpha(\hat{\boldsymbol{r}},\hat{\boldsymbol{r}}_s,\omega)F_\alpha(\hat{\boldsymbol{r}}_s,\omega)\mathrm{d}\Sigma, \tag{10}$$

where Σ is the unit sphere.

The cross spectrum Φ of background surface waves between stations $\boldsymbol{r}_1$ and $\boldsymbol{r}_2$ can be given by

$$\begin{aligned}\Phi(\boldsymbol{r}_1,\boldsymbol{r}_2,\omega) &= \langle \boldsymbol{u}(\boldsymbol{r}_1,\omega)\boldsymbol{u}^*(\boldsymbol{r}_2,\omega)\rangle \\ &= \mathcal{D}_L^1\mathcal{D}_L^2\Phi_{LL}(\hat{\boldsymbol{r}}_1,\hat{\boldsymbol{r}}_2,\omega) + \mathcal{D}_R^1\mathcal{D}_R^2\Phi_{RR}(\hat{\boldsymbol{r}}_1,\hat{\boldsymbol{r}}_2,\omega) \\ &\quad + \mathcal{D}_L^1\mathcal{D}_R^2\Phi_{LR}(\hat{\boldsymbol{r}}_1,\hat{\boldsymbol{r}}_2,\omega) + \mathcal{D}_R^1\mathcal{D}_L^2\Phi_{RL}(\hat{\boldsymbol{r}}_1,\hat{\boldsymbol{r}}_2,\omega)\end{aligned} \tag{11}$$

where $*$ represents a complex conjugate, $\langle\rangle$ denotes an ensemble (statistical) average, an $\alpha\beta$ component of the cross spectrum $\Phi_{\alpha\beta}(\hat{\boldsymbol{r}}_1,\hat{\boldsymbol{r}}_2,\omega)$ is $\left\langle \chi_\alpha(\hat{\boldsymbol{r}}_1,\omega)\chi_\beta^*(\hat{\boldsymbol{r}}_2,\omega)\right\rangle$, and $\mathcal{D}_\alpha^i$ is the spatial derivative at point $\hat{\boldsymbol{r}}_i$. For simplicity, the $\alpha\beta$ component of the cross spectrum $\Phi_{\alpha\beta}(\hat{\boldsymbol{r}}_1,\hat{\boldsymbol{r}}_2,\omega)$ is evaluated below.

The cross spectrum $\Phi_{\alpha\beta}(\hat{\boldsymbol{r}}_1,\hat{\boldsymbol{r}}_2,\omega)$ can be written as follows:

$$\Phi_{\alpha\beta}(\hat{\boldsymbol{r}}_1,\hat{\boldsymbol{r}}_2,\omega)=\int_\Sigma\int_\Sigma G_\alpha(\hat{\boldsymbol{r}}_1,\hat{\boldsymbol{r}},\omega)G^*_\beta(\hat{\boldsymbol{r}}_2,\hat{\boldsymbol{r}}',\omega)\times\Psi_{\alpha\beta}(\hat{\boldsymbol{r}},\hat{\boldsymbol{r}}',\omega)\mathrm{d}\Sigma\mathrm{d}\Sigma',\tag{12}$$

where $\Psi_{\alpha\beta}$ is the cross spectrum of surface traction $\left\langle F_\alpha(\hat{\boldsymbol{r}},\omega)F^*_\beta(\hat{\boldsymbol{r}}',\omega)\right\rangle$ between points $\hat{\boldsymbol{r}}$ and $\hat{\boldsymbol{r}}'$. Assuming that the excitation sources of the background surface waves are spatially isotropic but heterogeneous, the cross spectrum $\Psi_{\alpha\beta}(\hat{\boldsymbol{r}}',\hat{\boldsymbol{r}}'',\omega)$ is expressed in the following form:

$$\Psi_{\alpha\beta}(\hat{\boldsymbol{r}}',\hat{\boldsymbol{r}}'',\omega)=\sqrt{\hat{\Psi}_{\alpha\beta}(\hat{\boldsymbol{r}}',\omega)\hat{\Psi}_{\alpha\beta}(\hat{\boldsymbol{r}}'',\omega)}\,h\left(1-\frac{|\hat{\boldsymbol{r}}'-\hat{\boldsymbol{r}}''|}{L(\hat{\boldsymbol{r}}',\omega)}\right),\tag{13}$$

where $\hat{\Psi}_{\alpha\beta}(\boldsymbol{r},\omega)$ is a power spectrum of surface traction at $\hat{\boldsymbol{r}}$ (Fukao et al., 2002; Nishida and Fukao, 2007), $L(\hat{\boldsymbol{r}}',\omega)$ is the frequency-dependent coherent length, and the function $h(x)$ is the Heviside step function.

The excitation mechanism of ambient noise from 0.05 to 0.2 Hz, known as microseisms, is firmly established. Microseisms are identified at the primary and double frequencies: the primary microseisms at around 0.08 Hz have been ascribed to the direct loading of ocean swell onto a sloping beach (Haubrich et al., 1963). The typical frequency of secondary microseisms at around 0.15 Hz is approximately double the typical frequency of ocean swells, indicating the generation of the former via nonlinear wave–wave interactions among the latter (Longuet-Higgens, 1950). In both cases of the excitation mechanisms, the correlation length L can be characterized by the wavelength of ocean swell, on the order of 300 m, which is expected to be much shorter than the wavelength of seismic surface waves.

Supposing that the correlation length $L(\omega)$ is much shorter than the typical wavelength of background surface waves at ω, the cross spectrum $\Phi_{\alpha\beta}$ can be simplified as follows:

$$\Phi_{\alpha\beta}(\hat{\boldsymbol{r}}_1,\hat{\boldsymbol{r}}_2,\omega)=4\pi^2\int_\Sigma\hat{\Psi}^e_{\alpha\beta}(\hat{\boldsymbol{r}},\omega)G_\alpha(\hat{\boldsymbol{r}}_1,\hat{\boldsymbol{r}})G^*_\beta(\hat{\boldsymbol{r}}_2,\hat{\boldsymbol{r}})\mathrm{d}\Sigma.\tag{14}$$

Here, the power spectrum of effective surface traction per unit wavenumber $\hat{\Psi}^e_{\alpha\beta}(\omega)$ is defined as follows:

$$\hat{\Psi}^e_{\alpha\beta}(\hat{\boldsymbol{r}},\omega)\equiv\frac{L^2(\hat{\boldsymbol{r}},\omega)}{4\pi R^2}\hat{\Psi}_{\alpha\beta}(\hat{\boldsymbol{r}},\omega).\tag{15}$$

3. 2-D Born sensitivity kernel for a CCF of background surface waves in the case of a heterogeneous source distribution

Employing a first-order Born approximation of a cross spectrum $\Phi_{\alpha\beta}$ (Eq. (14)), a 2-D Born sensitivity kernel is estimated for the cross spectrum, which is a representation of a CCF in the frequency domain.

The first-order perturbation of the cross spectrum $\delta\Phi$ can be written in terms of the perturbation of the Green's function δG, as follows:

$$\delta\Phi_{\alpha\beta}(\hat{\boldsymbol{r}}_1,\hat{\boldsymbol{r}}_2,\omega)=4\pi^2\int_\Sigma\hat{\Psi}^e_{\alpha\beta}(\hat{\boldsymbol{r}},\omega)\times\Big\{\delta G_\alpha(\hat{\boldsymbol{r}}_1,\hat{\boldsymbol{r}},\omega)G^*_\beta(\hat{\boldsymbol{r}}_2,\hat{\boldsymbol{r}},\omega)+G_\alpha(\hat{\boldsymbol{r}}_1,\hat{\boldsymbol{r}},\omega)\delta G^*_\beta(\hat{\boldsymbol{r}}_2,\hat{\boldsymbol{r}},\omega)\Big\}\mathrm{d}\Sigma.\tag{16}$$

δG_α can be written as follows (e.g. Yoshizawa and Kennett, 2005):

$$\delta G_\alpha(\hat{\boldsymbol{r}}_1,\hat{\boldsymbol{r}},\omega)=\int_\Sigma-2k^2_\alpha(\hat{\boldsymbol{r}}_3,\omega)\frac{\delta c(\hat{\boldsymbol{r}}_3,\omega)}{c(\hat{\boldsymbol{r}}_3,\omega)}G_\alpha(\hat{\boldsymbol{r}}_1,\hat{\boldsymbol{r}}_3)G_\alpha(\hat{\boldsymbol{r}}_3,\hat{\boldsymbol{r}})\mathrm{d}\Sigma_3.\tag{17}$$

The above equation can then be simplified as follows:

$$\delta\Phi_{\alpha\beta}(\hat{\boldsymbol{r}}_1,\hat{\boldsymbol{r}}_2,\omega)=\int_\Sigma K_{\alpha\beta}(\hat{\boldsymbol{r}}_1,\hat{\boldsymbol{r}}_2,\hat{\boldsymbol{r}}_3,\omega)\frac{\delta c(\hat{\boldsymbol{r}}_3,\omega)}{c(\hat{\boldsymbol{r}}_3,\omega)}\mathrm{d}\Sigma_3.\tag{18}$$

A 2-D Born sensitivity kernel for phase–velocity anomalies is defined as follows:

$$K_{\alpha\beta}(\hat{\boldsymbol{r}}_1,\hat{\boldsymbol{r}}_2,\hat{\boldsymbol{r}}_3,\omega)=-2\Big\{k^2_\alpha\Phi^*_{\beta\alpha}(\hat{\boldsymbol{r}}_2,\hat{\boldsymbol{r}}_3,\omega)G_\alpha(\hat{\boldsymbol{r}}_1,\hat{\boldsymbol{r}}_3)+k^2_\beta\Phi_{\alpha\beta}(\hat{\boldsymbol{r}}_1,\hat{\boldsymbol{r}}_3,\omega)G^*_\beta(\hat{\boldsymbol{r}}_2,\hat{\boldsymbol{r}}_3)\Big\}.\tag{19}$$

This form of the above equation is similar to that of an adjoint kernel (e.g. Tarantola., 1984; Tanimoto, 1990; Tromp et al., 2010). For example, the first term of the kernel can be represented by convolution in the time domain between the time reversal of the CCF and the propagating Green's function from $\hat{\boldsymbol{r}}_2$ to $\hat{\boldsymbol{r}}_3$.

4. 2-D Born sensitivity kernel in a spherically symmetric Earth model for a homogeneous source distribution

For simplicity, the focus is on 2-D Born sensitivity kernels in a spherically symmetric Earth model for a homogeneous source distribution. A scalar Green's function in a homogeneous model can be simplified in the following form:

$$G_\alpha(\hat{\boldsymbol{r}}_1,\hat{\boldsymbol{r}}_2,\omega)=\sum_l\left(\frac{2l+1}{4\pi(\xi^2_\alpha-l(l+1))}\right)P_l(\cos\Theta_{12}),\tag{20}$$

where Θ_{12} is the angular distance between $\hat{\boldsymbol{r}}_1$ and $\hat{\boldsymbol{r}}_2$, and P_l is the Legendre function of the l'th order.

In this section, it is assumed that homogeneous and isotropic sources excite background surface waves. This approximation enables us to simplify the α component of a cross spectrum in the following form:

$$\Phi_{\alpha\alpha}(\hat{\boldsymbol{r}}_1,\hat{\boldsymbol{r}}_2,\omega)=\hat{\Psi}^e_{\alpha\alpha}(\omega)\pi\sum_l\frac{2l+1}{(\xi^2_\alpha-l(l+1))(\xi^{*2}_\alpha-l(l+1))}\times P_l(\cos\Theta_{12}).\tag{21}$$

The cross terms $\Phi_{\alpha\beta}$ are omitted for $\alpha\neq\beta$ because they take values of zero in the case of a homogeneous source distribution.

Figure 1 shows a typical example of the Born sensitivity kernel of a Rayleigh wave at 5.61 mHz with the source spectrum $\Psi^e_{\alpha\alpha}$ of an empirical model (Fukao et al., 2002). The sensitivity is concentrated within the first Fresnel zone. The figure also shows the side lobes of the kernel, which are suppressed when considering band-limited kernels (Yoshizawa and Kennett, 2005), as shown in the following section.

To obtain a more comprehensive form of the kernel, a far-field approximation of the Green's function and the CCF is considered. A far-field representation of Green's function

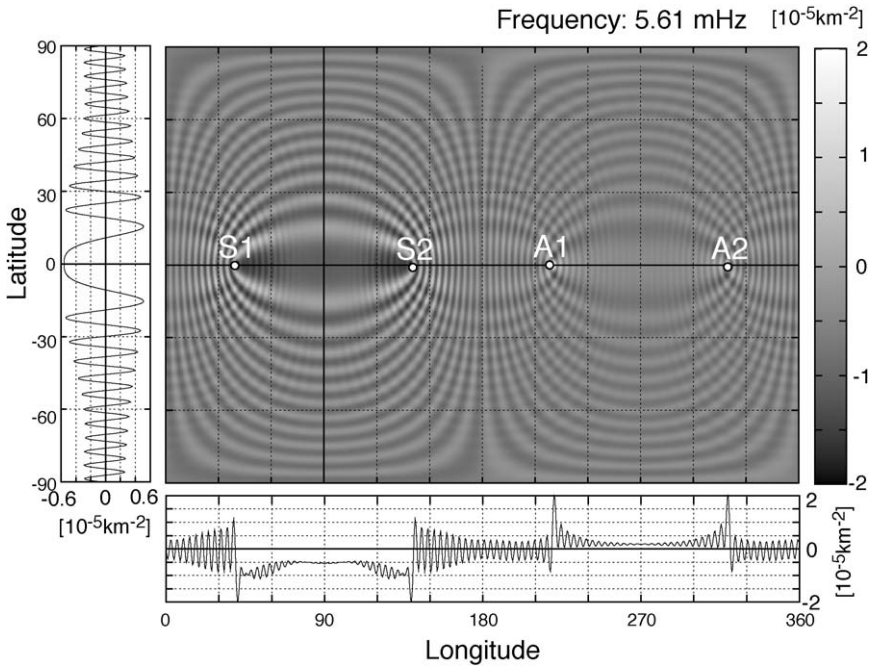

Fig. 1. Born sensitivity kernel of a Rayleigh wave at 5.61 mHz, with amplitude normalized by the cross spectrum $\Phi_{\alpha\alpha}(\Theta_{12},\omega)$. Each station is located on the equator. The longitude of station 1 is 40°; that of station 2 is 140°. The kernel was calculated using PREM (Dziewonski and Anderson, 1981). S1, S2, A1, and A2 indicate the locations of station 1, station 2, the antipode of station 1, and the antipode of station 2, respectively. This kernel is not singular, even near stations and near the antipodes of the stations.

Fig. 1. Noyau de sensibilité de Born d'une onde de Rayleigh à 5,61 mHz, d' amplitude normalisée par le spectre croisé $\Phi_{\alpha\alpha}(\Theta_{12},\omega)$. Chaque station est localisée sur l'Equateur. La longitude de la station 1 est 40°; celle de la station 2, 140°. Le noyau a été calculé en utilisant PREM (Dziewonski and Anderson, 1981). S1, S2, A1 et A2 indiquent la localisation de la station 1, de la station 2, l'antipode de la station 1 et l'antipode de la station 2, respectivement. Le noyau n'est pas singulier, même près des stations et des antipodes des stations.

is given as follows (Tromp and Dahlen, 1993):

$$G_\alpha(\hat{\mathbf{r}}_1,\hat{\mathbf{r}}_2,\omega)=\sum_{s=1}^{\infty} g_\alpha^s(\Delta_{12}^s,\omega). \tag{22}$$

The Green's function of the s'th orbit g_α^s is defined as follows:

$$g_\alpha^s(\Delta_{12}^s,\omega)=\frac{e^{i\left(-k_\alpha\Delta_{12}^s+(s-1)\frac{\pi}{2}-\frac{\pi}{4}\right)}e^{-\frac{\omega\Delta_{12}^s}{2C_\alpha Q_\alpha}}}{\sqrt{8\pi k_\alpha\sin|\Delta_{12}^s|}}, \tag{23}$$

where the integer $s(=1,2,\ldots)$ represents the surface wave orbits. The quantity Δ_{12}^s, which is the total angular distance traversed by a given arrival, is given by explicitly by,

$$\Delta_{12}^s=\begin{cases}\Theta_{12}+(s-1)\pi, s\,\text{odd}\\ s\pi-\Theta_{12}, s\,\text{even}.\end{cases} \tag{24}$$

Similarly to the approximation of the Green's function (Dahlen and Tromp, 1998, chapter 11.1), a far-field representation of the CCF is evaluated. Using the Poisson sum formula (Dahlen and Tromp, 1998, eq. 11.4, p. 408) to convert the summation over the angular degree l to an integral over the wavenumber k, the following representation is obtained:

$$\Phi_{\alpha\alpha}(\hat{\mathbf{r}}_1,\hat{\mathbf{r}}_2,\omega)=\hat{\Psi}^e_{\alpha\alpha}(\omega)\pi\sum_{s=-\infty}^{\infty}(-1)^s \times\int_0^\infty\frac{2}{(\xi_\alpha^2-k^2)(\xi_\alpha^{*2}-k^2)}P_{k-\frac{1}{2}}e^{-2isk\pi}kdk. \tag{25}$$

The above equation is transformed into a traveling representation of the CCF (Dahlen and Tromp, 1998, chapter 11.2), as follows:

$$\Phi_{\alpha\alpha}(\hat{\mathbf{r}}_1,\hat{\mathbf{r}}_2,\omega)=2\hat{\Psi}^e_{\alpha\alpha}(\omega)\pi \times\left[\sum_{s=1,3,\ldots}^{\infty}(-1)^{(s-1)/2}\int_{-\infty}^{\infty}\frac{Q^{(1)}_{k-1/2}e^{-i(s-1)k\pi}}{(\xi_\alpha^2-k^2)(\xi_\alpha^{*2}-k^2)}kdk+\sum_{s=2,4,\ldots}^{\infty}(-1)^{s/2} \times\int_{-\infty}^{\infty}\frac{Q^{(2)}_{k-1/2}e^{-isk\pi}}{(\xi_\alpha^2-k^2)(\xi_\alpha^{*2}-k^2)}kdk\right]. \tag{26}$$

The analysis employs a relation of the transformation into a traveling wave representation (Dahlen and Tromp, 1998, appendix B.11), as follows:

$$P_{k-\frac{1}{2}}(\cos\Theta)=Q^{(1)}_{k-\frac{1}{2}}(\cos\Theta)+Q^{(2)}_{k-\frac{1}{2}}(\cos\Theta), \tag{27}$$

where $Q^{(1,2)}_{k-1/2}$ corresponds to waves propagating in the direction of increasing and decreasing Θ, respectively. The following equation is also employed (Dahlen and Tromp,

1998, eq. 11.13):

$$Q^{(1,2)}_{-k-\frac{1}{2}}(\cos\Theta) = e^{\pm 2ik\pi} Q^{(1,2)}_{k-\frac{1}{2}}(\cos\Theta) + e^{\pm ik\pi}\tan k\pi P_{k-\frac{1}{2}}(-\cos\Theta). \quad (28)$$

Following (Dahlen and Tromp, 1998, chapter 11.3), the far-field approximation of the CCF is obtained as follows:

$$\Phi_{\alpha\alpha}(\hat{\boldsymbol{r}}_1, \hat{\boldsymbol{r}}_2, \omega) = \sum_{s=1}^{\infty} \phi^s_\alpha, (\Delta^s_{12}, \omega), \quad (29)$$

where $\phi^s_\alpha(\Delta^s_{12}, \omega)$ is the cross spectrum of the s'th orbit, as follows:

$$\phi^s_\alpha(\Delta^s_{12}, \omega) = \hat{\Psi}^e_{\alpha\alpha}(\omega)\frac{2\pi^2 Q_\alpha C_\alpha}{\omega} \times \left\{ g^s_\alpha(\Delta^s_{12}, \omega) e^{\frac{\pi i}{2}} + g^{s*}_\alpha(\Delta^s_{12}, \omega) e^{-\frac{\pi i}{2}} \right\}. \quad (30)$$

Because the cross spectrum $\Phi_{\alpha\alpha}(\Theta_{12}, \omega)$ is a real function, the corresponding CCF is an even function, which has a causal part and an acausal part. The first term represents the causal part of the cross spectrum; the second term represents the acausal part. This equation shows the phase retreat ($\pi/2$) of the causal part of the corresponding CCF from the Green's function (Nakahara, 2006; Sanchez-Sesma and Campillo, 2006).

The symmetry between the causal and acausal parts is broken in the case of heterogeneous distribution of sources (Cupillard and Capdeville, 2010; Kimman and Trampert, 2010; Nishida and Fukao, 2007). Source heterogeneity also causes a bias of the phase from 0 to $\pi/4$ (Kimman and Trampert, 2010).

These far field representations were used to calculate an asymptotic 2-D Born sensitivity kernel $K^1_\alpha(\hat{\boldsymbol{r}}_1, \hat{\boldsymbol{r}}_2, \hat{\boldsymbol{r}}_3, \omega)$ for a minor arc propagation (R1 or G1), and $K^2_\alpha(\hat{\boldsymbol{r}}_1, \hat{\boldsymbol{r}}_2, \hat{\boldsymbol{r}}_3, \omega)$ for a major arc propagation (R2 or G2), as follows:

$$K^1_\alpha = -\frac{2\pi\hat{\Psi}^e_{\alpha\alpha} Q_\alpha C_\alpha / c_\alpha}{\sqrt{\sin\Theta_{13}\sin\Theta_{23}}} \sin\left(k_\alpha(\Theta_{13}+\Theta_{23})\right) e^{-\frac{\omega(\Theta_{13}+\Theta_{23})}{2Q_\alpha C_\alpha}} \quad (31)$$

$$K^2_\alpha = -\frac{2\pi\hat{\Psi}^e_{\alpha\alpha} Q_\alpha C_\alpha / c_\alpha}{\sqrt{\sin\Theta_{13}\sin\Theta_{23}}} \times \left(\cos\left(k_\alpha(\pi + \Theta_{1'3} + \Theta_{23})\right) e^{-\frac{\omega(\pi+\Theta_{1'3}+\Theta_{23})}{2Q_\alpha C_\alpha}} + \cos\left(k_\alpha(\pi + \Theta_{13} + \Theta_{2'3})\right) e^{-\frac{\omega(\pi+\Theta_{13}+\Theta_{2'3})}{2Q_\alpha C_\alpha}} - \sin\left(k_\alpha(2\pi + \Theta_{1'3} + \Theta_{2'3})\right) e^{-\frac{\omega(2\pi+\Theta_{1'3}+\Theta_{2'3})}{2Q_\alpha C_\alpha}} \right), \quad (32)$$

where Θ_{ij} is the angular distance between the i'th and j'th points, as shown in Fig. 2.

5. 2-D phase sensitivity kernel in a spherically symmetric Earth model for a homogeneous source distribution

To obtain a phase sensitivity kernel for phase–velocity perturbations, the causal part of an R1 or G1 wave packet $\phi^{c,1}_\alpha(\hat{\boldsymbol{r}}_1, \hat{\boldsymbol{r}}_2, ,\omega)$ is isolated as follows:

$$\phi^{c,1}_\alpha(\hat{\boldsymbol{r}}_1, \hat{\boldsymbol{r}}_2, \omega) = \frac{\hat{\Psi}^e_{\alpha\alpha}(\omega) 2\pi^2 Q_\alpha(\omega) C_\alpha(\omega)}{\omega} g^1_\alpha(\Theta_{12}, \omega) e^{\frac{\pi i}{2}}. \quad (33)$$

The causal part of the Born sensitivity kernel is defined as follows: $K^{c,1}_\alpha = \frac{1}{2}(K^1_\alpha - \mathcal{H}(K^1_\alpha)i)$, where $\mathcal{H}$ represents the Hilbert transform in the frequency domain. For simplicity, the source term $\hat{\Psi}^e_{\alpha\alpha}$ is assumed to be a smooth function in the frequency domain. Then, perturbation of the causal part $\delta\phi^{c,1}_\alpha$ can be written as

$$\delta\phi^{c,1}_\alpha = \int_\Sigma \frac{\delta c_\alpha(\hat{\boldsymbol{r}}_3, \omega)}{c_\alpha} K^{c,1}_\alpha(\hat{\boldsymbol{r}}_1, \hat{\boldsymbol{r}}_2, \hat{\boldsymbol{r}}_3, \omega) \mathrm{d}\Sigma_3. \quad (34)$$

The Rytov approximation is employed to obtain a phase sensitivity kernel for phase–velocity perturbations (e.g. Yoshizawa and Kennett, 2005; Zhou et al., 2004). In the Rytov method, the logarithm of the cross spectrum $\phi^{c,1}_\alpha$ is considered instead of the wavefield itself. By taking the logarithm, $\phi^{c,1}_\alpha$ can be divided into real (amplitude) and imaginary (phase) parts, as follows:

$$\ln\phi^{c,1}_\alpha = \ln\left(A^1_\alpha \exp\left(-\psi^1_\alpha i\right)\right) = \ln A^1_\alpha - \psi^1_\alpha i, \quad (35)$$

where A^1_α is the amplitude of the causal wave packet, and ψ^1_α is its phase. The phase perturbation $\delta\psi^1_\alpha$ for propaga-

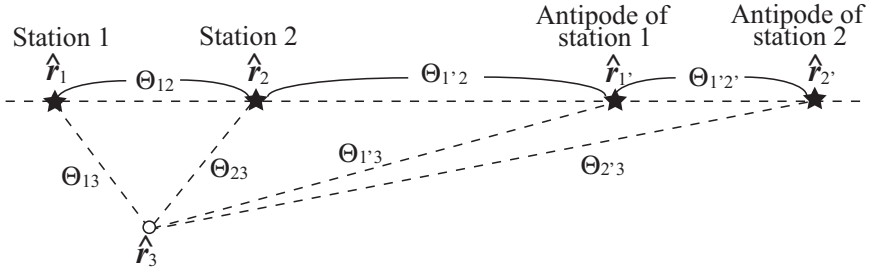

Fig. 2. Schematic map of the geometry of stations and their antipodes. Star symbols show the locations of stations at $\hat{\boldsymbol{r}}_1$ and $\hat{\boldsymbol{r}}_2$, and those of their antipodes at $\hat{\boldsymbol{r}}'_1$ and $\hat{\boldsymbol{r}}'_2$. The open circle shows the location of a phase velocity anomaly at $\hat{\boldsymbol{r}}_3$.

Fig. 2. Carte schématique de la géométrie des stations et de leurs antipodes. Les symboles en étoile montrent la localisation des stations à $\hat{\boldsymbol{r}}_1$ et $\hat{\boldsymbol{r}}_2$ et celle de leurs antipodes $\hat{\boldsymbol{r}}'_1$ et$\hat{\boldsymbol{r}}'_2$. Le cercle vide montre la localisation d'une anomalie de vitesse de phase à $\hat{\boldsymbol{r}}_3$.

tion along the minor arc (R1 or G1) is given by

$$\delta\psi_\alpha^1 = \int K_{p,\alpha}^1(\hat{\mathbf{r}}_1, \hat{\mathbf{r}}_2, \hat{\mathbf{r}}_3, \omega)\frac{\delta c}{c}\mathrm{d}\Sigma_3, \tag{36}$$

where the phase sensitivity kernel $K_{p,\alpha}^1$ is the imaginary part of $-K_\alpha^{c,1}/\phi_\alpha^{c,1}$.

Using the asymptotic kernel $K_\alpha^{c,1}$, a phase sensitivity kernel for R1 or G1 can be written as

$$K_{p,\alpha}^1 = -\frac{k_\alpha^{\frac{3}{2}}}{\sqrt{2\pi}}\left(\frac{\sin\Theta_{12}}{\sin\Theta_{13}\sin\Theta_{23}}\right)^{\frac{1}{2}} \times \cos\left(k_\alpha(\Theta_{13}+\Theta_{23}-\Theta_{12})-\frac{\pi}{4}\right)e^{-\frac{\omega(\Theta_{13}+\Theta_{23}-\Theta_{12})}{2Q_\alpha c_\alpha}}. \tag{37}$$

This expression of the phase sensitivity kernel is the same as that for phase measurements of earthquake data (Yoshizawa and Kennett, 2005). The equivalence of the expressions serves as validation of ambient noise tomography. Of course, this discussion is valid only under the assumptions of one-dimensional background structure and a homogeneous source distribution.

Actual phase-velocity anomalies are measured with a finite frequency band (e.g. Bensen et al., 2007). To consider a sensitivity kernel for phase measurements, an averaged phase-velocity kernel $\bar{K}_{p,\alpha}^1$ in a certain frequency band is better than that at a single frequency. An averaged kernel $\bar{K}_{p,\alpha}^1$ is defined as follows:

$$\bar{K}_{p,\alpha}^1 = \frac{1}{\Delta f}\int_{f_0-\Delta f/2}^{f_0+\Delta f/2} K_{p,\alpha}^1 \mathrm{d}f, \tag{38}$$

where f_0 is the central frequency and Δf is the frequency band width.

In the same manner, a phase sensitivity kernel $K_{p,\alpha}^2$ for R2 or G2 is given by

$$K_{p,\alpha}^2 = \frac{k_\alpha^{\frac{3}{2}}}{\sqrt{2\pi}}\left(\frac{\sin\Theta_{12}}{\sin\Theta_{13}\sin\Theta_{23}}\right)^{\frac{1}{2}} \times \left(\sin\left(k_\alpha(\Theta_{1'3}+\Theta_{23}-\Theta_{1'2})-\frac{\pi}{4}\right)e^{-\frac{\omega(\Theta_{1'3}+\Theta_{23}-\Theta_{1'2})}{2Q_\alpha c_\alpha}}\right. \tag{39}$$

$$\left. +\sin\left(k_\alpha(\Theta_{13}+\Theta_{2'3}-\Theta_{12'})-\frac{\pi}{4}\right)e^{-\frac{\omega(\Theta_{13}+\Theta_{2'3}-\Theta_{12'})}{2Q_\alpha c_\alpha}} - \cos\left(k_\alpha(\Theta_{1'3}+\Theta_{2'3}-\Theta_{12})-\frac{\pi}{4}\right)e^{-\frac{\omega(\Theta_{1'3}+\Theta_{2'3}-\Theta_{1'2'})}{2Q_\alpha c_\alpha}}\right). \tag{40}$$

It is also possible to define an averaged phase-velocity kernel $\bar{K}_{p,\alpha}^2$.

Figure 3 shows a typical example of the phase sensitivity kernels $\bar{K}_{p,\alpha}^1$ and $\bar{K}_{p,\alpha}^2$ at a central frequency of 7.5 mHz for a frequency band width of 5 mHz. The sensitivity is concentrated within the first Fresnel zones. The side lobes of the kernels are suppressed due to averaging in the frequency domain. The expression of the

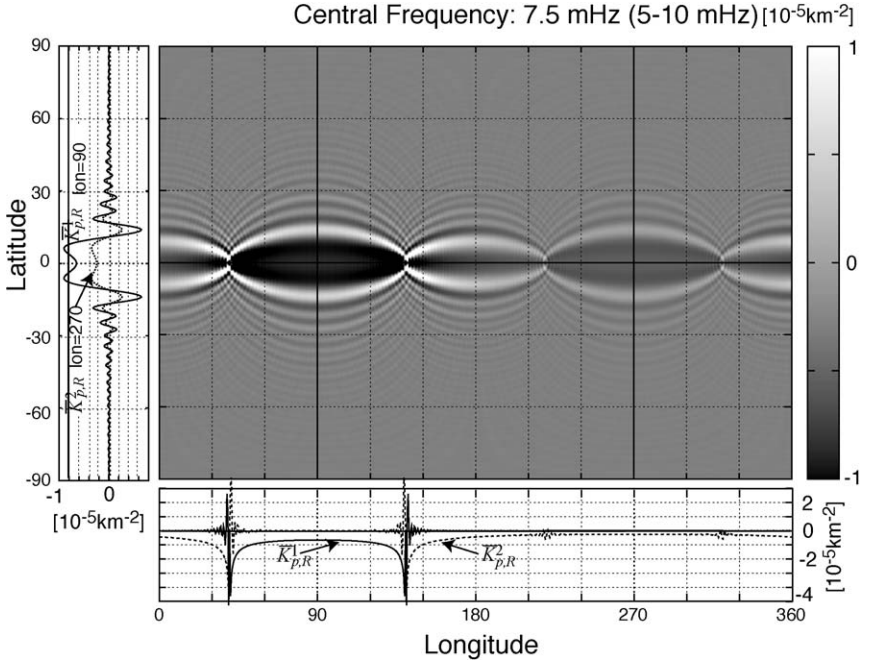

Fig. 3. Imaginary part of the Rytov sensitivity kernels ($\bar{K}_{p,\alpha}^1$ and $\bar{K}_{p,\alpha}^2$) of the fundamental Rayleigh wave at a central frequency of 7.5 mHz (from 5 to 10 mHz). Each station is located on the equator. The lower panel and the left-hand panel show slices of the kernels along the paths indicated by solid lines (an equatorial path, and the lines of longitude at 90° and 140°). The lower panel shows that the kernels have negative values along the minor and major arcs.
Fig. 3. Partie imaginaire des noyaux de sensibilité de Rytov ($\bar{K}_{p,\alpha}^1$ et $\bar{K}_{p,\alpha}^2$) du mode fondamental de l'onde de Rayleigh, à une fréquence centrale de 7,5 mHz (de 5 à 10 mHz). Chaque station est localisée sur l'Equateur. Le panneau inférieur et le panneau de gauche montrent des coupes des noyaux le long de trajets indiqués par des lignes continues (trajet équatorial et sur les lignes de longitude à 90° et 140°). Le panneau inférieur montre que les noyaux ont des valeurs négatives le long des arcs mineurs et majeurs.

R2 kernel is equivalent to that for earthquake data (Spetzler et al., 2002), which validates its application of ambient noise tomography using the observed phase-velocity anomalies of R2 data (Nishida et al., 2009).

6. Effects of heterogeneous distribution of sources on a Born sensitivity kernel

This section considers the effects of heterogeneous distribution of sources on the Born sensitivity kernel. For simplicity, the kernel K_α^1 is considered in a spherically symmetric case for the minor arc. It is simply assumed, phenomenologically, that the cross spectrum ϕ_α^1 has only azimuthal dependency, as follows:

$$\phi_\alpha^1(\Delta_{12}^1,\omega) = \hat{\Psi}_{\alpha\alpha}^e \frac{2\pi^2 Q_\alpha C_\alpha}{\omega}\Big(a(\varphi_{12}) g_\alpha^1(\Delta_{12}^1,\omega) e^{\frac{1}{2}\pi i} + a(\varphi_{21}) g_\alpha^{1*}(\Delta_{12}^1,\omega) e^{-\frac{1}{2}\pi i}\Big), \tag{41}$$

where $a(\varphi)$ is a real coefficient that varies as a function of azimuth, and φ_{12} is the back-azimuth to $\hat{\boldsymbol{r}}_2$ at $\hat{\boldsymbol{r}}_1$. Because the focus is on the perturbation of a time-symmetric part of a CCF, the real part of the Born sensitivity kernel K_α^1 is evaluated, as follows:

$$\Re[K_\alpha^1] \propto -\{a(\varphi_{23}) + a(\varphi_{13})\}\sin\left(k_\alpha(\Theta_{23}+\Theta_{13})\right) - \{a(\varphi_{23}) - a(\varphi_{13})\}\cos\left(k_\alpha(\Theta_{23}-\Theta_{13})\right), \tag{42}$$

where $\Re$ indicates the real part. The first term shows an elliptic pattern with foci at the stations, whereas the second term shows a hyperbolic pattern with foci at the stations. The second term vanishes in the case of a homogeneous source distribution, as in Eq. (31). If the time symmetry of the CCF is broken because of a heterogeneous source distribution, the second term would take on a hyperbolic pattern. Thus, the antisymmetry causes a bias in phase velocity maps, even without phase changes in the causal and acausal parts. Note that the second term vanishes in the case of $|\hat{\boldsymbol{r}}_3| \gg |\hat{\boldsymbol{r}}_2 - \hat{\boldsymbol{r}}_1|$.

Of course, the coefficient $a(\varphi)$ may have a imaginary part because an incomplete source distribution also causes a bias in the phase from 0 to $\pi/4$ (Kimman and Trampert, 2010). The imaginary part also causes a severe bias of the Born sensitivity kernel.

7. Conclusion

A theory of Born and phase sensitivity kernels was developed for a CCF using potential representation for surface waves. Simple forms were shown of Born and phase sensitivity kernels of a CCF in a spherically symmetric Earth model, assuming a homogeneous source distribution. The expression of the resultant phase sensitivity kernel is equivalent to that for phase measurements of earthquake data. This equivalence indicates the validity of ambient noise tomography under the given assumptions. The incomplete source distribution defines a hyperbolic pattern with foci at the pair of stations in a spherically symmetric case, which would generate a bias in the measured phase-velocity anomaly.

Acknowledgment

The author thanks Dr. Anne Seiminski, an anonymous reviewer, and the associate editor Dr. Michel Campillo for their constructive comments.

References

Bensen, G.D., Ritzwoller, M.H., Barmin, M.P., Levshin, A.L., Lin, F., Moschetti, M.P., Shapiro, N.M., Yang, Y., 2007. Processing seismic ambient noise data to obtain reliable broad-band surface wave dispersion measurements. Geophys. J. Int. 169, 1239–1260.

Bensen, G.D., Ritzwoller, M.H., Yang, Y., 2009. A 3D shear velocity model of the crust and uppermost mantle beneath the United States from ambient seismic noise. Geophys. J. Int. 177, 1177–1196.

Cupillard, P., Capdeville, Y., 2010. On the amplitude of surface waves obtained by noise correlation and the capability to recover the attenuation: a numerical approach. Geophys. J. Int. 181, 1687–1700.

Dahlen, F.A., Tromp, J., 1998. Theoretical Global Seismology. Princeton University Press, NJ, USA, 1025 p.

Dziewonski, A.M., Anderson, D.L., 1981. Preliminary reference Earth model. Phys. Earth. Planet. Inter. 25, 97–356.

Fukao, Y., Nishida, K., Suda, N., Nawa, K., Kobayashi, N., 2002. A theory of the Earth's background free oscillations. J. Geophys. Res. 107 (B9), 2206.

Haubrich, R., Munk, W., Snodgrass, F., 1963. Comparative spectra of microseisms and swell. Bull. Seismol. Soc. Am. 53, 27–37.

Kimman, W.P., Trampert, K., 2010. Approximations in seismic interferometry and their effects on surface waves. Geophys. J. Int. 182, 461–476.

Lin, F.C., Ritzwoller, M.H., Snieder, R., 2009. Eikonal Tomography: Surface wave tomography by phase-front tracking across a regional broad-band seismic array. Geophys. J. Int. 177, 1091–1110.

Longuet-Higgens, M.S., 1950. A theory of the origin of microseisms. Phil. Trans. Roy. Soc. London 243, 1–35.

Nakahara, H., 2006. A systematic study of theoretical relations between spatial correlation and Green's function in 1D, 2D and 3D random scalar wave fields. Geophys. J. Int. 167, 1097–1105.

Nishida, K., Fukao, Y., 2007. Source distribution of Earth's background free oscillations. J. Geophys. Res. 112, B06306.

Nishida, K., Kawakatsu, H., Obara, K., 2008. Three-dimensional crustal S-wave velocity structure in Japan using microseismic data recorded by Hi-net tiltmeters. J. Gephys. Res. 113, B10302.

Nishida, K., Montagner, J.P., Kawakatsu, H., 2009. Global Surface Wave Tomography Using Seismic Hum. Science 326, 112.

Sanchez-Sesma, F.J., Campillo, M., 2006. Retreival of the Green function from cross-correlation: the canonical elastic problem. Bull. Seismol. Soc. Am. 96, 1182–1191.

Shapiro, N., Campillo, M., Stehly, L., Ritzwoller, M., 2005. High-Resolution Surface-Wave Tomography from Ambient Seismic Noise. Science 307, 1615–1618.

Snieder, R., 2004. Extracting the Green's function from the correlation of coda waves: A derivation based on stationary phase. Phys. Rev. E 69, 046610.

Spetzler, J., Trampert, J., Snieder, R., 2002. The effect of scattering in surface wave tomography. Geophys. J. Int. 149, 755–767.

Tanimoto, T., 1990. Modelling curved surface wave paths; membrane surface wave synthetics. Geophys. J. Int. 102, 89–100.

Tarantola, A., 1984. Inversion of seismic reflection data in the acoustic approximation. Geophysics 49, 1259–1266.

Tromp, J., Dahlen, F.A., 1993. Variational principles for surface wave propagation on a laterally heterogeneous Earth–III, Potential representation. Geophys. I. Int. 112, 195–209.

Tromp, J., Luo, Y., Hanasoge, S., Peter, D., 2010. Noise cross-correlation sensitivity kernels. Geophys. J. Int. 183, 791–819.

Yoshizawa, K., Kennett, B.L.N., 2005. Sensitivity kernels for finite-frequency surface waves. Geophys. J. Int. 162, 910–926.

Zhou, Y., Dahlen, F.A., Nolet, G., 2004. Three-dimensional sensitivity kernels for surface wave observables. Geophys. J. Int. 158, 142–168.